

# Dynamics of the eye's wave aberration

**Heidi Hofer**

*Center for Visual Science, University of Rochester, Rochester, New York 14627*

**Pablo Artal**

*Laboratorio de Optica, Universidad de Murcia, Campus de Espinardo (Edificio C), 30071 Murcia, Spain*

**Ben Singer**

*Center for Visual Science, University of Rochester, Rochester, New York 14627*

**Juan Luis Aragón**

*Laboratorio de Optica, Universidad de Murcia, Campus de Espinardo (Edificio C), 30071 Murcia, Spain*

**David R. Williams**

*Center for Visual Science, University of Rochester, Rochester, New York 14627*

Received December 23, 1999; revised manuscript received August 21, 2000; accepted September 12, 2000

It is well known that the eye's optics exhibit temporal instability in the form of microfluctuations in focus; however, almost nothing is known of the temporal properties of the eye's other aberrations. We constructed a real-time Hartmann–Shack (HS) wave-front sensor to measure these dynamics at frequencies as high as 60 Hz. To reduce spatial inhomogeneities in the short-exposure HS images, we used a low-coherence source and a scanning system. HS images were collected on three normal subjects with natural and paralyzed accommodation. Average temporal power spectra were computed for the wave-front rms, the Seidel aberrations, and each of 32 Zernike coefficients. The results indicate the presence of fluctuations in all of the eye's aberration, not just defocus. Fluctuations in higher-order aberrations share similar spectra and bandwidths both within and between subjects, dropping at a rate of approximately 4 dB per octave in temporal frequency. The spectrum shape for higher-order aberrations is generally different from that for microfluctuations of accommodation. The origin of these measured fluctuations is not known, and both corneal/lenticular and retinal causes are considered. Under the assumption that they are purely corneal or lenticular, calculations suggest that a perfect adaptive optics system with a closed-loop bandwidth of 1–2 Hz could correct these aberrations well enough to achieve diffraction-limited imaging over a dilated pupil. © 2001 Optical Society of America

*OCIS codes:* 330.7310, 330.5370, 330.6130.

## 1. INTRODUCTION

The eye's wave aberration and corresponding point-spread function are not static but fluctuate over time. The eye's focus exhibits fluctuations about its mean level during steady-state accommodation with amplitudes of approximately 0.03–0.5 diopters (D) and with temporal frequencies up to 5 Hz.<sup>1</sup> The amplitude and frequency characteristics of these fluctuations depend on conditions such as mean accommodation level, pupil diameter, and target form.<sup>1</sup> Though these microfluctuations have been characterized in many studies, almost nothing is known about the stability of the other monochromatic aberrations such as coma and spherical aberration. Microfluctuations in accommodation are thought to be large enough to affect retinal image quality, yet small enough that they probably produce little if any perceptible effect on vision under normal circumstances.<sup>1</sup> We sought to determine whether other aberrations also change over time and whether these changes are large enough to have important consequences for vision or for imaging the retina.

The ability to measure higher-order aberrations of the eye raises the possibility of correcting them with a static compensating method, such as a customized contact lens, an intraocular lens, or an improved procedure for laser refractive surgery. The effectiveness of such static methods will be limited by the dynamics of the eye's wave aberration.

The characterization of these dynamics is especially important in the design of systems that can correct aberrations in real time. Liang *et al.*<sup>2</sup> compensated the eye's wave aberration with a deformable mirror, providing a transverse resolution high enough that individual photoreceptors could be seen and classified in the living eye.<sup>3</sup> However, this system, as well as other correction attempts,<sup>4,5</sup> were incapable of correcting changes in the wave aberration faster than several minutes. Further increases in image quality might be achieved with an adaptive optics system that tracked and compensated these changes in real time, as is often done to remove the effects of atmospheric turbulence in ground-based telescopes.<sup>6</sup> Such a system could also eliminate the need

to use cycloplegic drugs, which are sometimes used to reduce the temporal variation in refractive state.

Previous methods of measuring the eye's wave aberration, such as the spatially resolved refractometer,<sup>7</sup> the aberroscope,<sup>8</sup> phase retrieval from double-pass images,<sup>9</sup> or initial versions of the Hartmann–Shack (HS) wave-front sensor,<sup>10,11</sup> can measure only the static properties of the wave aberration. Liang<sup>12</sup> described a wave-front sensor that operated at video rates but did not use it to characterize the temporal changes in the eye's wave aberration. We describe a new wave-front sensor for the eye that can automatically measure the wave aberration at temporal frequencies up to 60 Hz, providing the first characterization of the temporal fluctuations of the eye's aberrations beyond defocus.

## 2. METHODS

### A. Experimental Setup

We modified a HS wave-front sensor to make measurements of the eye's wave aberration at 25 Hz. Figure 1 shows a diagram of the apparatus. A collimated infrared (780 nm) beam is focused on the retina. The use of infrared light increases the amount of light reflected by the retina and is more comfortable and safe for the subjects, while the estimates of the image quality are similar to those obtained by using visible light.<sup>13</sup> The light reflected from the retina is used to measure the wave aberration. The eye's pupil is conjugate with a microlens array in which each lenslet has a 0.6-mm diameter and a 40-mm focal length. A CCD camera (Dalsa CA-D4) placed in the focal plane of the microlens array records the HS images. A focus corrector stage, consisting of a pair of mirrors that could be translated between two achromats of a Badal system, was used to bring the retina in focus on the CCD camera. The irradiance on the cornea was lower than 40  $\mu\text{W}$ , approximately five times less than the maximum permissible exposure for continuous viewing for this wavelength, according to the American National Standards Institute standards for the safe use of lasers.<sup>14</sup>

A polarizing beam splitter was initially used to remove

the corneal reflection from the HS image. At the time when our HS wave-front sensor was first constructed, the polarizing beam splitter was our favored method of removing the corneal reflection from the HS images. Since then we have come to favor a different method, the off-axis illumination method, for removing the corneal reflection. With the off-axis method, the HS laser beacon enters the eye's pupil at a position displaced approximately 1 mm from the pupil center, which causes the corneal reflection to be displaced in the retinal plane. By placing a suitable stop in a retinal conjugate plane, one can block the corneal reflection from the HS image. The off-axis method improves the homogeneity of the HS spots in addition to increasing the amount of light available for the HS image. Because no polarizing beam splitter is used, none of the light returning from the retina is rejected from the HS spot image. Approximately halfway through the current study, we inserted a quarter-wave plate into the system to undo the state of crossed polarization induced by the polarizing beam splitter. This was an expedient way to achieve the benefits of the off-axis method with our system.<sup>15</sup>

The higher the temporal bandwidth of a wave-front sensor, the more susceptible it is to noise. For exposures less than a few seconds and even at high light levels, the HS images are degraded by spatial noise, which reduces the accuracy of the wave aberration measurement. This spatial noise has multiple causes. The reflectance of the retina illuminated by the laser beacon is spatially nonuniform as a result of, for example, the grain of the photoreceptor mosaic, variations in reflectance of individual receptors, and variations in the reflectance of layers both in front of and behind the receptors. In addition, when the retina is illuminated in coherent light, speckle is produced by the interference of light scattered from different locations within the three-dimensional retinal tissue. This noise is not problematic for long exposures because eye movements move the retina with respect to the laser spot, spatially averaging the noise. But noise becomes progressively worse as exposure time is shortened below approximately, 1 s, and considerably shorter exposure times ( $< \sim 80$  ms) are required to measure the temporal properties of the eye's wave aberration.

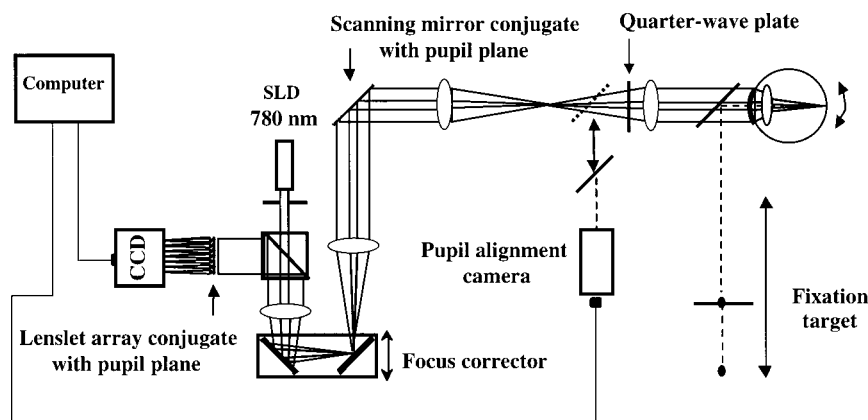


Fig. 1. Experimental apparatus. Light from the SLD (1-mm beam size) enters the eye, forming a diffraction-limited spot on the retina. This light scatters from the retina, passes through the eye's optics, and emerges as an aberrated wave front in the pupil plane. The microlens array, which is conjugate with the pupil plane, collects the light and forms a HS spot image on the CCD. The scanning mirror, conjugate with the pupil, scans the laser spot across the retina at 600 Hz. Because the same light is also descanned, there is no movement of the spots on the CCD camera, or of the light distribution in the pupil plane with respect to the microlens array.

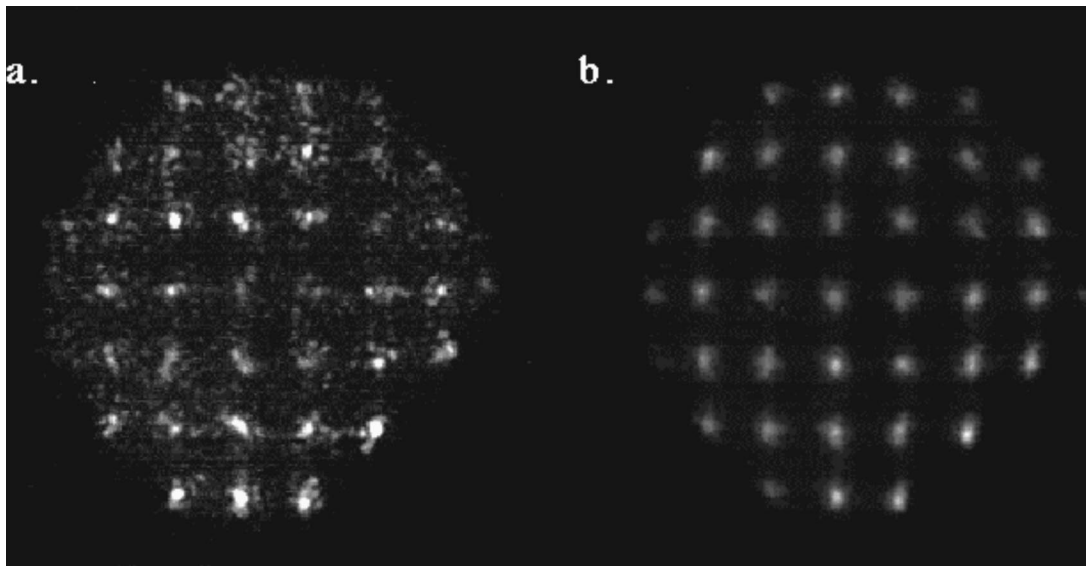


Fig. 2. HS images taken (a) without and (b) with the scanning mirror. Both images were taken under identical conditions with a He-Ne laser and 20-ms exposure on the same human subject. Spot compactness and uniformity are much better in (b) than in (a).

We used three approaches to reduce noise in the HS images. First, to reduce laser speckle, we used a low-coherence light source, a 780-nm superluminescent diode (SLD), instead of a laser. This SLD has a spectral bandwidth of approximately 20 nm, and a coherence length of approximately 30  $\mu\text{m}$  compared with approximately 1 m for a He-Ne laser. The shorter coherence length diminishes the interference effects of light scattered from different locations within the retina and reduces speckle in the HS images. Second, we used a scanning system to further reduce spatial noise. A scanning mirror placed in a plane conjugate with the entrance pupil of the eye scans the laser spot across a portion of the retina at 600 Hz, spatially averaging the noise and further smoothing the HS images. Since the same scanning mirror also descans the light returning from the eye, movement of the scanning spot is confined to the retina. There is no movement of the wave front in the pupil plane or of the HS spots on the CCD camera. We found that a movement of 15–30 arc min was sufficient to remove most of the spatial noise from the images. With this scanning amplitude, noise in the measurement of the Zernike coefficients is decreased by approximately a factor of 2. Figure 2 shows an example of the benefit of the scanning system when used with coherent light. With these modifications, good-quality HS images are recorded at rates limited only by the speed of the camera, currently approximately 60 Hz. Finally, the insertion of the quarter-wave plate into the system between the scanning mirror and the eye slightly improves the homogeneity of the HS spots on the CCD in addition to increasing the total amount of light for the measurement severalfold.

## B. Procedure

### 1. Data Acquisition

Measurements were performed on three trained subjects (the authors), whose age and refraction were as follows: HH, 23, sphere +1.25 D, cylinder 0.75 D; JA, 25, sphere

+1 D, cylinder 2.75 D; and PA, 37, sphere  $-2\text{D}$ . JA was corrected with trial lenses for astigmatism; the other subjects were left uncorrected. Light from the fixation target entered through the subject's entire natural pupil, and light exiting the entire pupil was collected for the HS images. The subject's eye was aligned with the entrance pupil of the system with the use of a video camera coupled into the system by inserting a mirror just before the last lens in the system. The optical axis of the video camera corresponded to the optical axis of the wave-front sensor. After the initial pupil alignment, the subject was stabilized with a bite bar and instructed to bring the HS laser beacon into focus by moving the focus corrector stage. For those trials where subjects viewed a target, subjects were instructed to accommodate on the target and focus the HS laser beacon by moving the focus corrector stage until the laser spot appeared to be in focus in the same plane as that of the target.

Measurements of the eye's wave aberration were made under several different conditions with paralyzed and unparalyzed accommodation. For unparalyzed accommodation (natural viewing), measurements were made while the subject accommodated on a complex target at 3.3 D, 2 D, and the far point. The target was coupled into the system by using a pellicle beam splitter inserted just before the entrance pupil of the system. Accommodation was controlled by varying the physical distance between the target and the entrance pupil. For those measurements made at the subjects' far point, a lens was introduced into the system, and the target was placed at the position behind the lens appropriate for each observer. (For a perfectly emmetropic subject, this position would be one focal length behind the lens.) Data for all the natural accommodation conditions were typically taken in the same session. For each subject, data were also taken after accommodation had been paralyzed with either two drops of cyclopentolate (HH and JA) or two drops of tropicamide (PA). For each condition, eight series of 128 HS images were acquired with a duration of 5 s at 25.6 Hz.

Subjects were instructed to maintain accurate accommodation and fixation throughout each image sequence.

## 2. Data Processing: Hartmann–Shack Spot Centroiding and Wave-Front Reconstruction

Despite our efforts to minimize spatial inhomogeneity of the HS spots on the CCD, residual noise causes error in the detection of the spot centroids. These problems are exacerbated somewhat by the lower light levels in short-exposure images. We developed a robust subpixel pyramidal search algorithm capable of automatically detecting the centroids of the HS spots in all of our series of images. With this algorithm, the centroid location of each HS spot is iteratively evaluated in windows of decreasing size, each centered on the previous estimate. The initial windows are boxes centered on the reference array positions with the same widths as the interlenslet spacing. When the final window size is reached, centroid location is determined by performing a subpixel average. Empirically, we found that the most accurate and repeat-

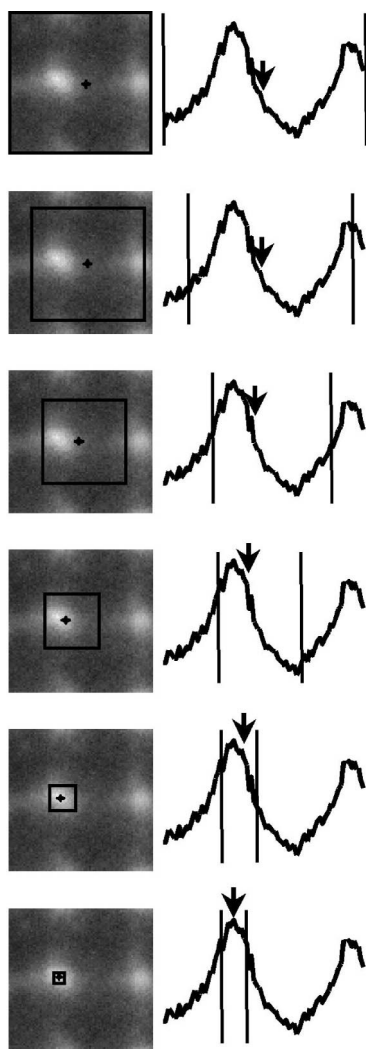


Fig. 3. Illustration of the centroiding algorithm. The top panel shows the centroiding error that would be obtained with a simple algorithm that determines spot centroids by computing the center of mass within each search box. Successive panels show the result of the new algorithm after each iteration, until finally in the bottom panel the spot centroid is accurately determined.

able centroid detection, for images such as ours, occurred when the size of the last window was roughly comparable with the width of the diffraction pattern from a single subaperture. This iterative procedure helps to prevent nonuniformities outside the core of the spot from influencing the centroid calculation. Figure 3 presents an example of the performance of the centroiding algorithm. From the set of spot displacements, the wave front was reconstructed as an expansion of Zernike polynomials<sup>16</sup> by a matrix inversion method.

For each series of images, the Zernike decomposition of the wave aberration was computed for pupil diameters of 4.7 and 5.8 mm encompassing 37 and 57 HS spots, respectively. Empirically, we found that the largest Zernike order that we could use in the decomposition and still obtain stable and reliable fits was up to fifth order for the 4.7-mm pupil (37 lenslets) and up to seventh order for the 5.8-mm pupil (57 lenslets). For the natural viewing conditions without cycloplegia, the maximum pupil size that could be used was limited by the subject's physical pupil size. In these cases, the Zernike decomposition could not always be computed for the larger pupil size.

Temporal power spectra were calculated for the fluctuations in the total rms wave-front error, the Seidel aberrations, and each of the Zernike coefficients by using a 128-point discrete Fourier transform algorithm. Power spectra of all the series within each condition were averaged to obtain power spectra for each subject for the different conditions and pupil sizes. Because of our 5-s duration and 25.6-Hz sampling rate, we were unable to acquire data for frequencies below 0.2 Hz or above 12.8 Hz. Average spectra for Zernike coefficients of various radial orders were computed by averaging the spectra of all the Zernike coefficients within a particular order.

## 3. RESULTS AND DISCUSSION

### A. Temporal Variations of the Eye's Aberrations

Figure 4 shows typical data for the temporal variations in the eye's aberrations for a 4.7-mm pupil size. The traces show the variation in one subject's total rms wave-front error and some of the Zernike aberrations during steady-state accommodation at approximately 2 D. The ordinate is the value of the aberration in micrometers, and the abscissa is time in seconds. Zernike coefficient sequences such as these were used in the temporal power spectra computations.

To ensure that the measurement process did not introduce spectral artifacts, we took data for an artificial eye consisting of a photographic objective (reversed to maximize aberrations) with a black diffuser acting as an artificial retina. The objective was purposely misaligned and defocused to obtain HS images that were similar in signal level and in quality to those of human eyes. The variation measured in the total rms wave-front error for a perfectly static artificial eye is also shown in Fig. 4, with the trace vertically displaced for clarity.

Spectra for the total rms wave-front error for the artificial eye and a human eye are shown in Fig. 5. The spectrum of the artificial eye is nearly flat and very low in magnitude, lying well below that for the real eye. This is true for artificial eyes both with and without the scanning

mirror and for varying levels of signal in the HS images, indicating that spectral artifacts were not introduced by the instrument or the data analysis. The difference in the artificial and real eye spectra at a comparable light level illustrates that photon noise and CCD read noise are not responsible for the temporal behavior that we observe in the real eye. In general, random noise in the measurement would be expected to produce a flat spectrum in the real eye rather than the negatively sloping function that we observed.

Figure 6 shows how the fluctuations of the total rms wave-front error are distributed among different Zernike radial orders for one subject with paralyzed accommodation.

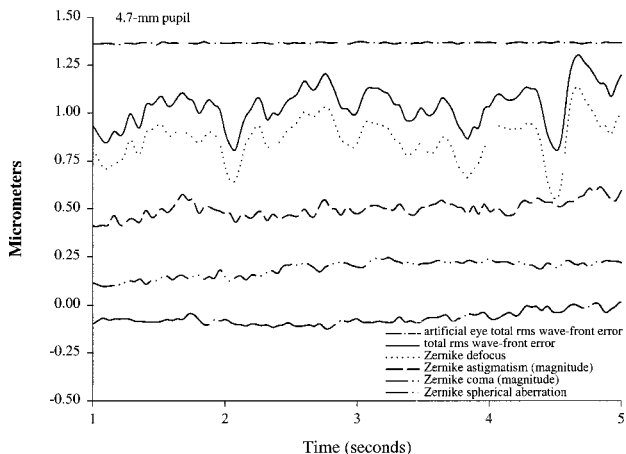


Fig. 4. Temporal traces of the total rms wave-front error, the coefficient of the Zernike defocus term, the magnitude of the Zernike astigmatism terms, the magnitude of the Zernike coma terms, and the coefficient of the Zernike spherical aberration term for subject HH when accommodating on a target at 2 D. For reference, a trace showing the variation in the total rms wave-front error for an artificial eye is included at the top of the plot. All aberrations were computed for a 4.7-mm pupil size.

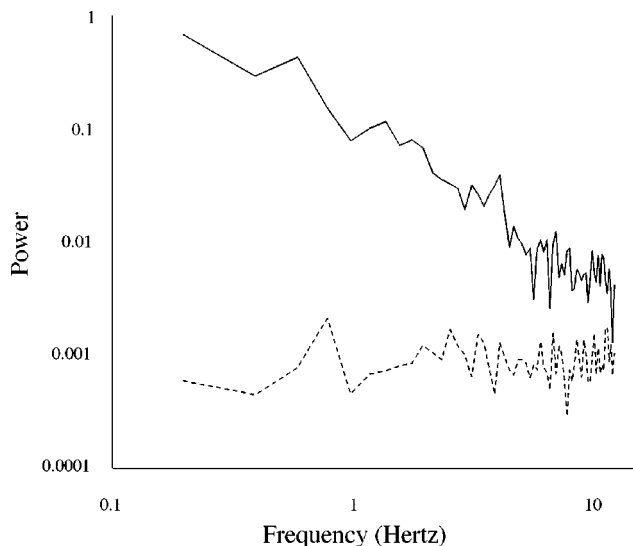


Fig. 5. Comparison of the power spectrum of the fluctuations in the total rms wave-front error for an artificial eye and for a human subject with paralyzed accommodation. Aberrations were computed for a 4.7-mm pupil size. The solid curve shows the spectrum for the human eye, and the dashed curve shows the power spectrum for the artificial eye. Both the power and frequency axes are logarithmic.

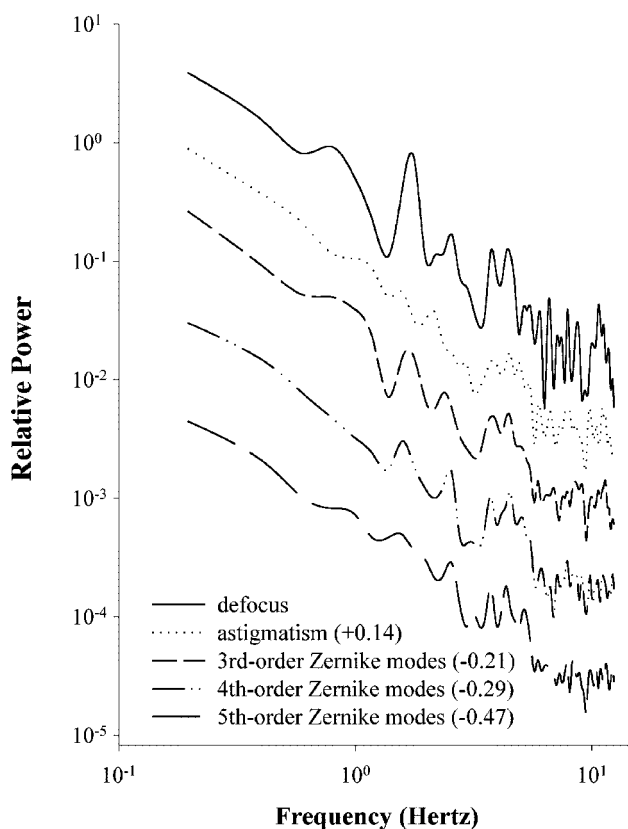


Fig. 6. Averaged power spectra for Zernike modes of different orders for a human subject with paralyzed accommodation. Aberrations were computed for a 4.7-mm pupil size. The scale on the ordinate is applicable only to the curve for defocus; the spectra for the fluctuations in astigmatism and those for the higher orders of aberration have been vertically shifted for clarity. The numbers in parentheses next to the descriptions of the curves indicate the original power of these fluctuations, in log units, relative to those of defocus.

tion. Each curve represents the average power spectrum of the fluctuations in all of the Zernike modes within a given order. Plots have been shifted on the log-power axis to allow better comparison. The spectra are similar for all the Zernike orders, falling with approximately the 4/3 power of frequency (or 4 dB per octave). All spectra have measurable power out to approximately 5–6 Hz. The results for the two other subjects are similar.

## B. Origin of Fluctuations in the Eye's Aberrations

### 1. Relationship to Microfluctuations

One possibility for the origin of the fluctuations in aberrations other than defocus is that they are a direct consequence of microfluctuations of accommodation. Support for this hypothesis comes from evidence that large changes in accommodative state produce systematic changes in other aberrations in the eye. (Full results of the changes in the wave aberration with accommodation are to be published in a future paper.) For example, Fig. 7 shows, for two subjects, that large voluntary changes in focus of the eye produce systematic changes in spherical aberration. However, three lines of evidence suggest that microfluctuations in accommodation are not the primary cause of the fluctuations in other aberrations. First, it is possible to predict the amplitude of the fluctua-

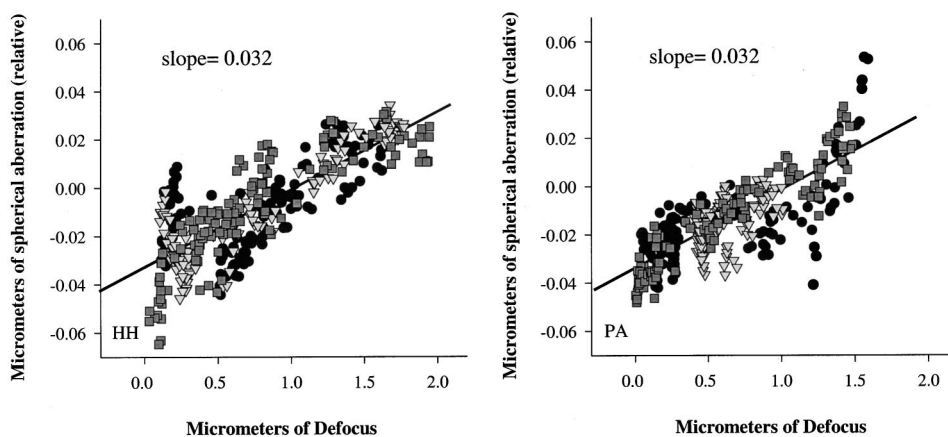


Fig. 7. Relationship between accommodative state and spherical aberration for HH and PA. Plots show the measurement results from three trials in which the subjects voluntarily changed their accommodation over a range of approximately 2 D within a 5-s interval. Zero defocus represents the subject's far point. Each point on the graph is the Zernike coefficient of spherical aberration plotted against the Zernike coefficient of defocus for one of the 128 measurements made during the 5-s interval of each trial. The three different symbols within each plot indicate individual points taken from each of the three separate measurements. For better slope comparison, the values of spherical aberration have been plotted for each subject relative to that subject's value of spherical aberration when accommodating at 1 D (which was approximately the middle of the accommodative range over which measurements were taken). The lines indicate the best-fitting linear regression curves for each subject; the slopes of these lines are indicated on the plots.

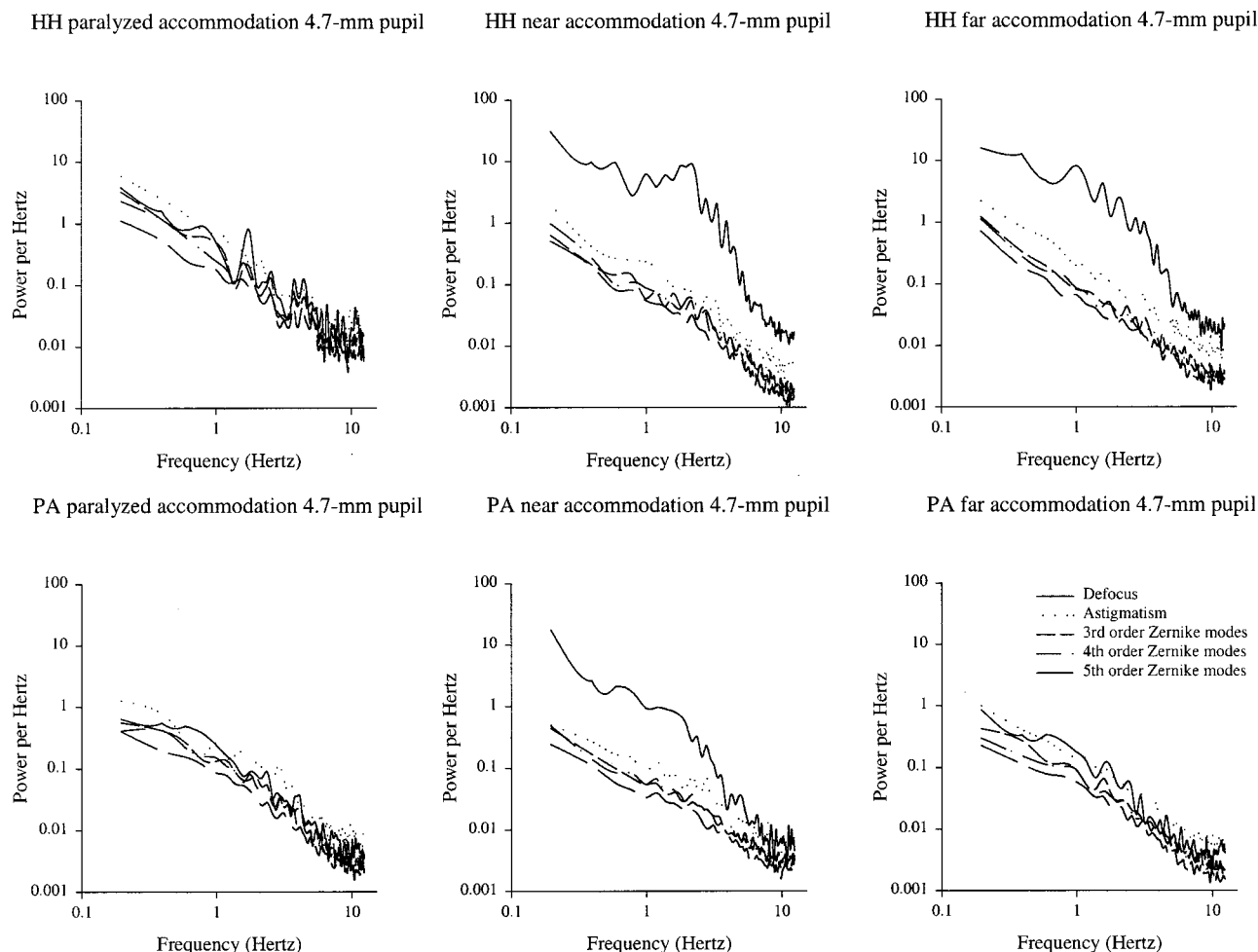


Fig. 8. Averaged power spectra of the fluctuations in defocus, astigmatism, and the third-, fourth-, and fifth-order Zernike modes for subjects HH and PA for the conditions of (a) paralyzed accommodation and natural accommodation on (b) near and (c) far targets.

tions in other aberrations expected from focus variations by using measurements such as those in Fig. 7. For example, for both HH and PA, a  $0.1\text{-}\mu\text{m}$  change in defocus, which is typical of microfluctuations in accommodation, corresponds to a change in spherical aberration of only  $0.0032\ \mu\text{m}$ . But this value is ten times smaller than the observed fluctuation in spherical aberration. Second, if accommodative microfluctuations were driving changes in other aberrations, we would expect to observe correlations between them. We examined average correlation matrices for each subject, condition, and pupil size and found no systematic correlations. Third, the hypothesis predicts that the suppression of microfluctuations with cycloplegia should cause a corresponding suppression of the fluctuations in other aberrations. Figure 8 shows the power spectra for different-order Zernike modes for (a) paralyzed accommodation, (b) natural viewing on a near (3.3-D) target, and (c) natural viewing on a far target for two subjects. As expected, the microfluctuations in accommodation are more powerful when viewing a near target with natural accommodation than with paralyzed accommodation; however, the fluctuations in the higher Zernike orders are not decreased by cycloplegia for these two subjects.

## 2. Eye Movements

Another possible cause for the fluctuations is that they are artifacts produced by eye movements. There are at least two kinds of movements to consider: rotation and translation of the eye. Rotation of the eye is caused by fixational eye movements. These are very small, on the order of  $3\ \text{arc min}^{17}$  for a carefully fixating eye and are therefore unlikely to correspond to significant changes in the wave aberration. Some evidence for this comes from examination of retinal images of the cone mosaic obtained with adaptive optics.<sup>3</sup> The quality of these images does not change across the  $1\text{-deg}$  field of view of the instrument, which is many times larger than the fixation instability. We gathered further support that the eye's wave aberration does not differ significantly over a fairly large rotational field by taking data on the dynamics of the eye's aberrations while asking the subject to make deliberate rotational eye movements, on the order of  $0.5\ \text{deg}$ . The results of these measurements were similar to those made while the subject was carefully fixating.

Translation during the measurement is caused by small instabilities in head position on the bite bar and because of very small changes in fixation. Fluctuations that are due to pupil translation will not affect a person's visual performance in ordinary viewing conditions. However, they will reduce image quality in any system using an artificial pupil, especially, for example, an adaptive optics system for high-resolution retinal imaging. To estimate the fluctuations attributable to pupil translation, in a separate study, we measured pupil translation<sup>18</sup> in two subjects, finding an amplitude of  $0.1\ \text{mm}$ . We then computed the effect that this translation would have on a measured wave aberration (for PA), assuming that the only source of variability was pupil translation. This computation was performed by taking the average wave aberration measured for PA over a  $7\text{-mm}$  pupil, then truncating the wave aberration to a  $4.7\text{-mm}$  pupil cen-

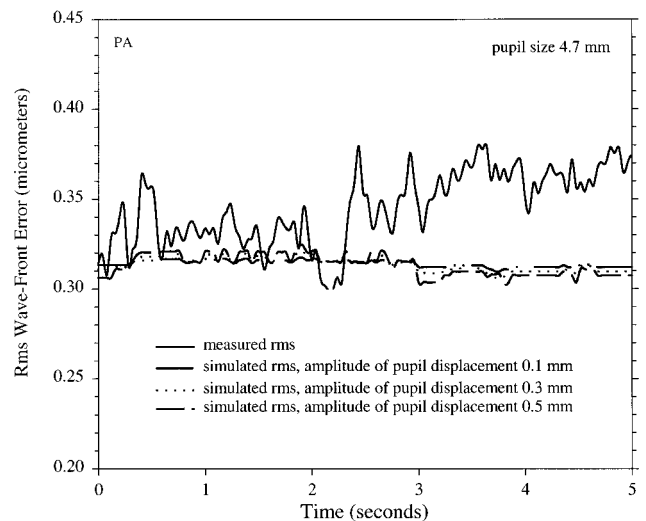


Fig. 9. Simulated effect of pupil translation. The solid curve shows the actual variation measured during a typical trial in PA's total rms wave-front error computed for a  $4.7\text{-mm}$  pupil size. The various dotted and dashed curve show the expected variation that one would measure in total rms wave-front error if the wave front were perfectly stable but the pupil center were moving with different amplitudes of displacement.

tered on a translated pupil, and performing a numerical decomposition of this new wave aberration into new Zernike coefficients. This was done for each of 128 pairs of horizontal and vertical pupil displacements that were taken from the data of Miro *et al.*<sup>18</sup> for the pupil movement during 5 s. The result of this simulation was 128 sets of Zernike coefficients describing how the measured coefficients for PA's static wave aberration would have changed over 5 s had PA's pupil been moving with the translations that were applied in the simulation. These simulations, and also simulations with the amplitude of the pupil movement scaled up to  $0.3$  and  $0.5\ \text{mm}$ , were compared with the actual dynamics that were measured for a  $4.7\text{-mm}$  pupil during a typical 5-s trial for PA. Figure 9 shows that the predicted variation, for pupil movement with an amplitude of  $0.1\ \text{mm}$ , in the rms wave aberration is 16 times smaller than the actual variation that we measured. Indeed, even translational movements with amplitudes as large as  $0.5\ \text{mm}$ , which we would have clearly seen in the HS image sequences, were incapable of producing fluctuations as large as those measured. We conclude that neither eye rotation nor pupil translation artifacts are major sources of the fluctuations that we measure in the eye's wave aberration.

## 3. Other Possible Sources of the Fluctuations

Other possible causes for the fluctuations include local changes in tear film thickness over the cornea, perhaps caused by evaporation, blinking, or eye movements, and instabilities in the lens. The spectral signature of the heartbeat is a temporal frequency component at  $1\text{--}1.5\ \text{Hz}$  ( $60\text{--}90$  beats per minute), which we could see occasionally. Changes in the axial length of the eye caused by the heartbeat are approximately  $4\ \mu\text{m}$ ,<sup>19</sup> or only  $0.01\ \text{D}$ , approximately one order of magnitude smaller than the variations in defocus that we report here, even with paralyzed accommodation.

Though we have excluded a number of potential causes for the fluctuations in the wave aberration, such as instrument artifact, random noise, and direct optical effects of eye rotation and translation, our experiments to date

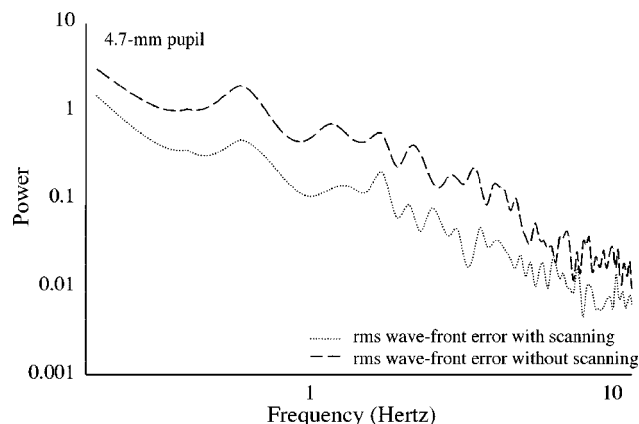


Fig. 10. Power spectra for fluctuations in total rms wave-front error with and without the scanning mirror averaged across two subjects. The curves are nearly parallel, demonstrating that spatial inhomogeneity in real eyes does not act as a random noise source but causes a multiplicative increase in the power spectra of the measured fluctuations in the wave aberration.

have not identified the origin of the fluctuations in the eye with certainty. Nor have we demonstrated that the fluctuations that we measure produce corresponding fluctuations in the quality of the retinal image. We cannot exclude the possibility that they reflect changes in the properties of the beacon reflected from the retina rather than the properties of the eye's optics. For example, when the beacon is not deliberately scanned on the retina, spatial inhomogeneity in the fundus causes a multiplicative increase in the apparent fluctuation of the wave aberration at all temporal frequencies (see Fig. 10). Apparently, as the retina moves beneath the beacon, and perhaps because light is reflected from multiple retinal layers, the centroids of the HS spots can move relative to each other, even in the absence of changes in the wave aberration. Increasing the scanning amplitude beyond 30 arc min has virtually no additional effect on the HS images, leading us to believe that we have successfully removed the majority of the spatial inhomogeneity. Still, we have no certain method of determining the extent of residual spatial inhomogeneity in our images or its impact on the variability of the wave aberration. Therefore the fluctuation reported here should be considered an upper bound on the true dynamics of the wave aberration that might influence retinal image quality.

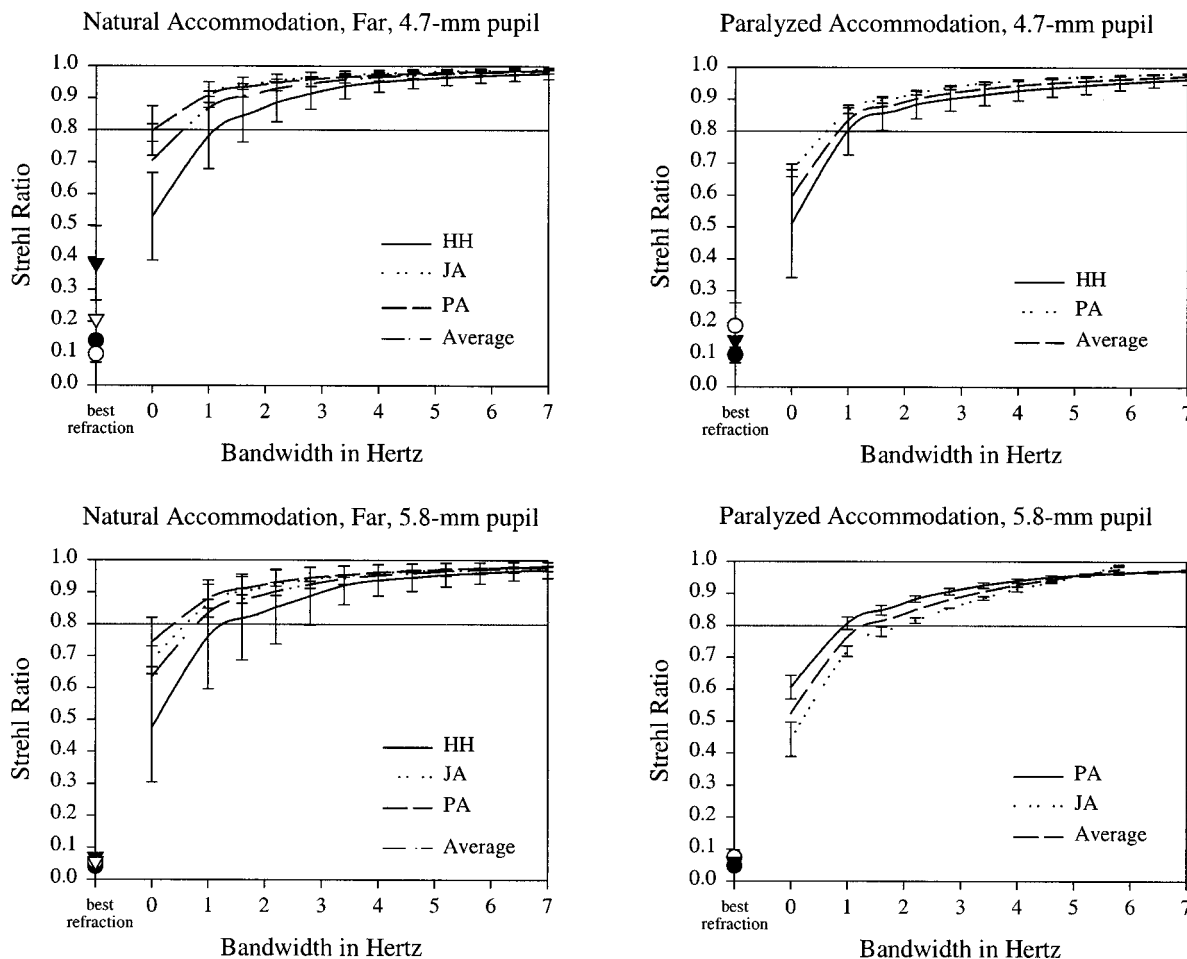


Fig. 11. Time-averaged Strehl ratio versus bandwidth for a perfect adaptive optics system, calculated for 4.7- and 5.8-mm pupils for paralyzed accommodation and for natural accommodation on a far target. Error bars on each subject's curve represent the standard deviations of the calculated results for that subject. Values of Strehl ratio higher than 0.8 are considered to correspond to diffraction-limited imaging.



### C. Implications of the Temporal Variations of the Aberrations on Adaptive Optics System Performance

Additional insight into the retinal versus corneal/lenticular causes of these fluctuations awaits a real-time adaptive optics system. Such a system will provide improved image quality only if the fluctuations are corneal or lenticular, leading to changes in retinal image quality. For now, we assume that none of the fluctuations is caused by retinal effects and compute the bandwidth that an adaptive optics system would require to correct these fluctuations. This result will provide an upper bound on the actual bandwidth required. To estimate the image quality of the eye coupled to an adaptive optics system, we use the Strehl ratio,<sup>20</sup> defined as the ratio of the peak height of the actual point-spread function to the height of a diffraction-limited point-spread function. A value of 0.8 or above is considered diffraction limited. We calculated the time-averaged Strehl ratio as a function of the bandwidth of a perfect adaptive optics system. The results of these calculations for two different pupil sizes are plotted in Fig. 11.

For paralyzed accommodation and a 5.8-mm pupil size (close to typical experimental conditions for adaptive optics applications), a perfect static correction, which corresponds to zero bandwidth, affords a tenfold improvement over a perfect conventional refraction (only defocus and astigmatism corrected). This is just slightly more than halfway to diffraction-limited performance and the best that can be attained with any static correction. To realize diffraction-limited performance, we require an adaptive optics system with a bandwidth of approximately 1.3 Hz. The range for the two subjects is 1–2 Hz. This does not mean that the eye does not exhibit fluctuations beyond frequencies of 1–2 Hz. It simply means that for this pupil size and this condition, the power carried by the fluctuations in frequencies above 1–2 Hz is too small to significantly impact image quality. It is estimated that closed-loop correction with adaptive optics requires a sampling rate at least 10–20 times the bandwidth of the fluctuations that are to be corrected, implying that an adaptive optics system operating at 10–40 Hz would be able to track all the significant fluctuations in the eye's aberrations for this pupil size. The results for unparalyzed accommodation on a distant target are similar. This similarity may seem surprising until it is remembered that the wave aberrations of these subjects exhibited remarkable stability, comparable with the stability in the paralyzed accommodation case, with unparalyzed accommodation by using a distant fixation target (see Fig. 8). Recently, with the Rochester second-generation adaptive optics system using a sampling rate of 21 Hz, we have been able to reduce the power in the fluctuations in the eye's aberrations up to fifth order with a correction bandwidth of approximately 0.8 Hz, decreasing the average residual rms wave-front error after correction by approximately a factor of 2. Results with the new device will be reported elsewhere.

For smaller pupil sizes (<4.7 mm), the effect of the fluctuations in the eye's wave aberration is less severe. Often, diffraction-limited performance could be achieved with a perfect static correction of all of the eye's aberrations, and in all cases a perfect static correction could af-

ford substantial gains over a perfect conventional refraction. These results imply that a customized static correction of the eye's wave aberration, such as with a custom contact lens, would still have utility in many normal-viewing situations despite the temporal fluctuations in the ocular aberrations.

### ACKNOWLEDGMENTS

This research was supported by National Institutes of Health grants EY0436, EY0139, and EY07125 (Research to Prevent Blindness) and Spanish Dirección General de Enseñanza Superior grant PB97-1056. When this research was carried out, P. Artal was on sabbatical in Rochester, partially supported by the Spanish Ministry of Education. J. L. Aragón acknowledges a fellowship from Fundacion Seneca, Murcia (Spain). H. Hofer acknowledges a National Science Foundation graduate fellowship.

Address correspondence to Heidi Hofer at the location on the title page or by phone, 716-275-8143 or e-mail, heidi@optics.rochester.edu.

### REFERENCES

1. W. N. Charman and G. Heron, "Fluctuations in accommodation: a review," *Ophthalmic Physiol. Opt.* **8**, 153–163 (1988).
2. J. Liang, D. R. Williams, and D. T. Miller, "Supernormal vision and high-resolution retinal imaging through adaptive optics," *J. Opt. Soc. Am. A* **14**, 2884–2892 (1997).
3. A. Roorda and D. R. Williams, "The arrangement of the three cone classes in the living human eye," *Nature (London)* **397**, 520–522 (1999).
4. F. Vargas-Martin, P. Prieto, and P. Artal, "Correction of the aberrations in the human eye with liquid crystal spatial light modulators: limits to the performance," *J. Opt. Soc. Am. A* **15**, 2552–2562 (1998).
5. A. W. Dreher, J. F. Bille, and R. N. Weinreb, "Active optical depth resolution improvement of the laser tomographic scanner," *Appl. Opt.* **24**, 804–808 (1989).
6. J. W. Hardy, "Active optics: a new technology for the control of light," *Proc. IEEE* **66**, 651 (1978).
7. M. S. Smirnov, "Measurement of the wave aberration of the human eye," *Biophysics (USSR)* **6**, 776–794 (1961).
8. H. C. Howland and B. Howland, "A subjective method for the measurement of monochromatic aberrations of the eye," *J. Opt. Soc. Am.* **67**, 1508–1518 (1977).
9. I. Iglesias, E. Berrio, and P. Artal, "Estimates of the ocular wave aberration from pairs of double-pass retinal images," *J. Opt. Soc. Am. A* **15**, 2466–2476 (1998).
10. J. Liang, B. Grimm, S. Goelz, and J. F. Bille, "Objective measurement of the wave aberrations of the human eye using a Hartmann–Shack wavefront sensor," *J. Opt. Soc. Am. A* **11**, 1949–1957 (1994).
11. J. Liang and D. R. Williams, "Aberrations and retinal image quality of the normal human eye," *J. Opt. Soc. Am. A* **14**, 2873–2883 (1997).
12. J. Liang, "A new method to precisely measure the wave aberrations of the human eye with a Hartmann–Shack wavefront sensor," Ph.D. dissertation (University of Heidelberg, Heidelberg, Germany, 1991).
13. N. Lopez-Gil and P. Artal, "Comparison of double-pass estimates of the retinal image quality obtained with green and near infrared light," *J. Opt. Soc. Am. A* **14**, 961–971 (1997).
14. *American National Standard for the Safe Use of Lasers*, ANSI Z136.1 (Laser Institute of America, Orlando, Fla., 1993).

15. H. J. Polland, Technolas, Munich, Germany (personal communication, March 25, 1999).
16. R. J. Noll, "Zernike polynomials and atmospheric turbulence," *J. Opt. Soc. Am.* **66**, 207–211 (1976).
17. R. W. Ditchburn, *Eye-Movements and Visual Perception* (Clarendon, Oxford, UK, 1973).
18. I. Miro, N. Lopez-Gil, and P. Artal, "Pupil meter and tracking system based in a fast image processing algorithm," in *Ophthalmic Technologies IX*, P. O. Rol, K. M. Joos, F. Manns, B. E. Stuck, and M. Belkin, eds., Proc. SPIE **3591**, 63–70 (1999).
19. L. F. Schmetterer, F. Lexer, C. J. Unfried, H. Sattmann, and A. F. Fercher, "Topical measurement of fundus pulsations," *Opt. Eng.* **34**, 711–716 (1995).
20. M. Born and E. Wolf, *Principles of Optics* (Pergamon, New York, 1985).